Cell Reports

Report

SARS-CoV-2 genomic surveillance identifies naturally occurring truncation of ORF7a that limits immune suppression

Graphical abstract

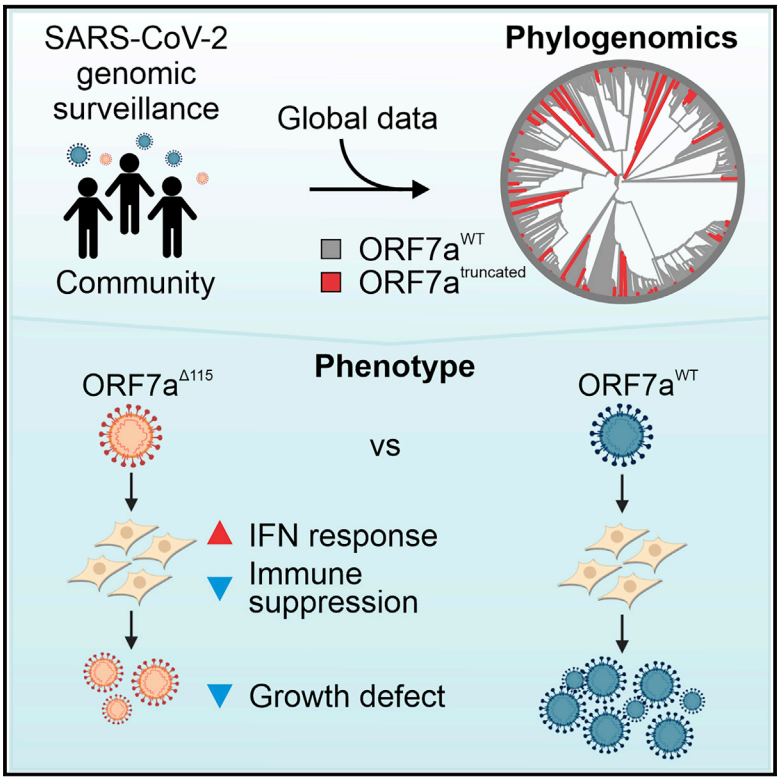

Highlights

- ORF7a mutations are found in SARS-CoV-2 genomes isolated from around the globe
- The ORF7aΔ115 isolate displays a replication defect
- An ORF7a mutation limits viral suppression of the interferon response

Authors

Artem Nemudryi, Anna Nemudraia, Tanner Wiegand, ..., Diane Bimczok, Mark A. Jutila, Blake Wiedenheft

Correspondence

bwiedenheft@gmail.com

In brief

Nemudryi et al. use global SARS-CoV-2 phylogenomics to identify mutations that frequently occur in the C-terminal end of ORF7a accessory protein. They isolate one of these mutant viruses from a patient sample and demonstrate that ORF7a truncation affects viral mechanisms responsible for suppressing host immune response.

Nemudryi et al., 2021, Cell Reports *35*, 109197
June 1, 2021 © 2021 The Author(s).
https://doi.org/10.1016/j.celrep.2021.109197

CellPress

Cell Reports

CellPress
OPEN ACCESS

Report

SARS-CoV-2 genomic surveillance identifies naturally occurring truncation of ORF7a that limits immune suppression

Artem Nemudryi,[1,3,5] Anna Nemudraia,[1,5] Tanner Wiegand,[1,6] Joseph Nichols,[1,6] Deann T. Snyder,[1] Jodi F. Hedges,[1] Calvin Cicha,[1] Helen Lee,[1] Karl K. Vanderwood,[2] Diane Bimczok,[1] Mark A. Jutila,[1] and Blake Wiedenheft[1,4,7,*]
[1]Department of Microbiology and Immunology, Montana State University, Bozeman, MT 59717, USA
[2]Gallatin City-County Health Department, Bozeman, MT 59715, USA
[3]Twitter: @artemnemudryi
[4]Twitter: @WiedenheftLab
[5]These authors contributed equally
[6]These authors contributed equally
[7]Lead contact
*Correspondence: bwiedenheft@gmail.com
https://doi.org/10.1016/j.celrep.2021.109197

SUMMARY

Over 950,000 whole-genome sequences of severe acute respiratory syndrome coronavirus 2 (SARS-CoV-2) have been determined for viruses isolated from around the world. These sequences are critical for understanding the spread and evolution of SARS-CoV-2. Using global phylogenomics, we show that mutations frequently occur in the C-terminal end of ORF7a. We isolate one of these mutant viruses from a patient sample and use viral challenge experiments to link this isolate (ORF7a$^{\Delta 115}$) to a growth defect. ORF7a is implicated in immune modulation, and we show that the C-terminal truncation negates anti-immune activities of the protein, which results in elevated type I interferon response to the viral infection. Collectively, this work indicates that ORF7a mutations occur frequently, and that these changes affect viral mechanisms responsible for suppressing the immune response.

INTRODUCTION

The spillover of severe acute respiratory syndrome coronavirus 2 (SARS-CoV-2) into the human population has resulted in a global pandemic of coronavirus disease 2019 (COVID-19) with more than 2.8 million deaths worldwide (https://coronavirus.jhu.edu/) (Andersen et al., 2020). Although much of the research on this virus is focused on the Spike protein, recent reports demonstrate that accessory proteins of SARS-CoV-2 might be involved in COVID-19 pathogenesis by modulating antiviral host responses (Young et al., 2020; Zhang et al., 2020). SARS-CoV-2 uses multiple strategies to evade host immunity. Accessory proteins ORF3b, ORF6, and ORF7a antagonize various steps of type I interferon (IFN-I) production and signaling, while the proposed function of ORF8 is downregulating antigen presentation (Konno et al., 2020; Lei et al., 2020; Miorin et al., 2020; Tan et al., 2020; Xia et al., 2020). To occlude signal transmission from IFN receptors, ORF7a subverts phosphorylation of STAT2, suppressing transcriptional activation of antiviral IFN-stimulated genes (ISGs) that can otherwise restrict viral replication (Martin-Sancho et al., 2020; Xia et al., 2020). Although the proposed function for ORF7a is intracellular, antibodies against ORF7a are elevated in the serum of COVID-19 patients (Hachim et al., 2020). Work that is currently under review indicates that recombinant ORF7a protein interacts with CD14^{+} monocytes and triggers expression of pro-inflammatory cytokines, including interleukin-6 (IL-6) and tumor necrosis factor alpha (TNF-α) (Zhou et al., 2021). However, it is unclear if these interactions happen in COVID-19 patients. Together, these data suggest that ORF7a plays a dual role in SARS-CoV-2 infection by modulating both the IFN and inflammatory responses.

Here, we show that C-terminal mutations in ORF7a occur frequently in samples isolated from patients around the globe. These mutations are not derived from a single lineage, and they do not persist over time. Using samples collected from infected patients, we have isolated a virus containing a deletion mutation in ORF7a that truncates the C-terminal half of the protein. *In vitro* viral challenge experiments demonstrate that this mutation results in a replication defect and obviates viral suppression of the immune response. Collectively, these data suggest that ORF7a truncations are defective in suppressing the host immune response, which may explain why these mutations quickly disappear in the immunocompetent population.

RESULTS

SARS-CoV-2 genomic surveillance identifies truncations of ORF7a

Genome sequencing has been used to track the rise and spread of new SARS-CoV-2 lineages over the course of the pandemic

This is an open access article under the CC BY-NC-ND license (http://creativecommons.org/licenses/by-nc-nd/4.0/).

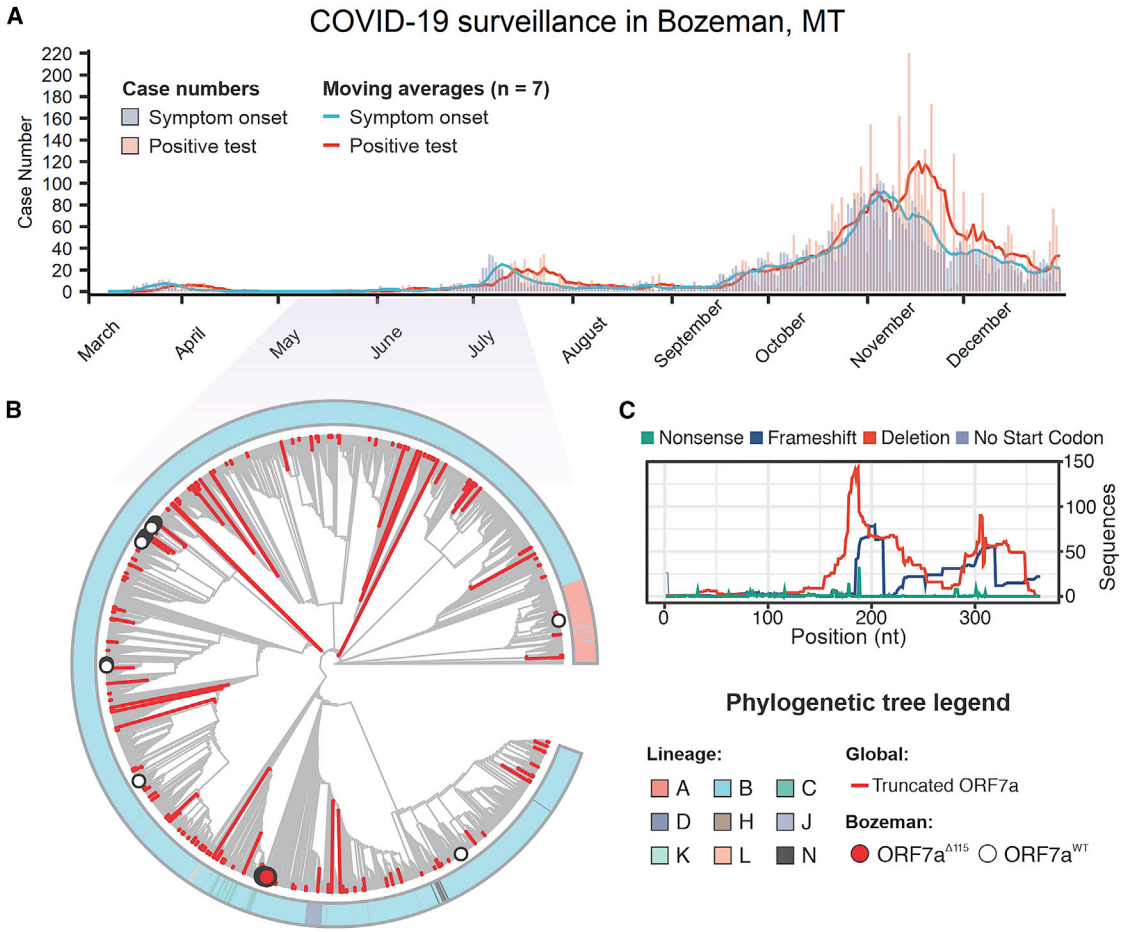

Figure 1. SARS-CoV-2 genomic surveillance identifies global reoccurrence of ORF7a truncations

(A) Symptom onset (purple) and PCR-based SARS-CoV-2 test results (coral) for patients in Bozeman, Montana, are shown with vertical bars. Seven-day moving averages, shown with lines, were used to indicate epidemiological trends.

(B) Phylogenetic analysis of SARS-CoV-2 genomes sampled in Bozeman and globally. The tree was constructed from an alignment of 55 Bozeman samples and 4,871 genomes subsampled from GISAID. Subsampling was performed using Augur utility (https://nextstrain.org) by selecting 10 genomes per country per month since the start of the pandemic. Outer ring shows SARS-CoV-2 lineages assigned to genome sequences (Rambaut et al., 2020a). Major lineages include A (pink) that is associated with initial outbreak in China and B (blue) that emerged later in Europe. Minor lineages (i.e., C-N) are offshoots of lineage B. Red branches identify truncated ORF7a variants (n = 205) detected in the global data and merged into the alignment. The red dot highlights 7 of the 55 ORF7a variants that were isolated in Bozeman between April and July (2020). White dots highlight 48 viral genomes isolated in Bozeman that have wild-type ORF7a sequences.

(C) Distribution of different mutations that occur along the ORF7a coding sequence.

(https://www.gisaid.org/) (Bedford et al., 2020; Korber et al., 2020). As part of this effort, we sequenced SARS-CoV-2 genomes isolated from patients in Bozeman, Montana (Figure 1A; Table S1). In total, we determined 55 whole-genome sequences of SARS-CoV-2 viruses isolated from patients between April and July 2020 using an amplicon-based Nanopore protocol from the ARTIC network (https://artic.network/) (Quick et al., 2017; Tyson et al., 2020). To place the local outbreak in the context of the global SARS-CoV-2 evolutionary trends, we aligned 55 whole-genome sequences isolated from patients in Bozeman to 4,235 genomes subsampled (10 genomes per month per country) from 181,003 SARS-CoV-2 genomes downloaded from the GISAID. The subsampling protocol removes redundancy and bias introduced by uneven distribution of the global SARS-CoV-2 sequencing effort. The resulting alignment was used to build a phylogenetic tree (Figure 1B). Of the 55 SARS-CoV-2 genomes determined from patients in Bozeman, only 1 was derived from the WA1 lineage (lineage A in Figure 1B) that was introduced to Washington state from Wuhan, China, in January 2020 (Bedford et al., 2020; Holshue et al., 2020). The remaining 54 genomes associate with clade B.1 and its offshoots, which are characterized by the D614G mutation in the spike and have prevailed globally since the spring of 2020 (Rambaut et al., 2020a) (Figure 1B). The genetic variability in SARS-CoV-2 circulating in Bozeman (April to July 2020) represents 14 independent viral lineages, reflecting multiple introductions of the virus to the community from many different sources (Figure S1A).

During the annotation of these genomes, we noticed a reoccurring (7 out of 55 genomes) 115-nt deletion in the gene-encoding accessory protein ORF7a (27,549–27,644 nt). The ORF7a$^{\Delta 115}$

mutation was found in patient swabs collected over a period of ~1.5 months (Table S1). RT-PCR and Sanger sequencing verified that all these seven ORF7a$^{\Delta 115}$ variants are bona fide mutations and not a sequencing artifact (Figures S1B and S1C). In addition to the ORF7a$^{\Delta 115}$ deletion, these genomes also share 10 single-nucleotide variants (SNVs) compared with the Wuhan-Hu-1 reference genome. Seven of the 10 SNVs are found frequently worldwide and are a signature of the B1.1 lineage of SARS-CoV-2 (Rambaut et al., 2020a). The remaining three mutations are rare, do not co-occur in any other genomes on GISAID, and lead to amino acid changes in ORF3a (Q38P, L95F) and N (R195I) proteins. Interestingly, one of the genomes in the ORF7a$^{\Delta 115}$ cluster has two additional SNVs that likely were acquired during circulation in the community. This virus was sampled from a patient 41 days after sampling the first ORF7a$^{\Delta 115}$ variant, which agrees well with estimated SARS-CoV-2 mutation rates (2 nt/month) (van Dorp et al., 2020).

To determine if the ORF7a$^{\Delta 115}$ genotype is unique to Bozeman, we downloaded an alignment of 180,971 SARS-CoV-2 genomes from GISAID, extracted ORF7a sequences, and determined their mutational profiles. In total, we identified 845 unique ORF7a gene variants that are different from the Wuhan-Hu-1 reference sequence. Next, we looked for mutations with major effect on the ORF7a amino acid sequence. We identified 189 unique ORF7a variants (825 total sequences) with frameshifts, deletions, or missense mutations causing premature stop codons (Figure 1C). To understand the evolutionary history of these mutations, we integrated these genome sequences into our phylogenetic analysis. Detected ORF7a variants appear to have emerged independently on every continent and were not confined to any single lineage (Figure 1B; Table S1). Next, we aligned translated ORF7a sequences to look for patterns. Most of the identified ORF7a mutations (126 out of 189) truncate the C terminus but preserve the N-terminal half of the protein (Figure 1C; Figure S1B). A portion (36.5%) of these truncated ORF7a variants appeared in two or more patient samples (116 maximum [max]). Although some of these ORF7a mutants appear to have arisen on multiple independent occasions, others come from genomes that form monophyletic clades, suggesting that viruses with ORF7a truncations are capable of transmission within a host population (Figure S1B).

ORF7a truncation has a loss-of-function effect

ORF7a is a type I transmembrane (TM) protein with an N-terminal immunoglobulin-like (Ig-like) ectodomain, stalk, TM domain, and short cytosolic tail (Figure 2A). The two β sheets of the ectodomain are held together by two disulfide bonds (i.e., Cys23-Cys58 and Cys35-Cys67) (Figure 2B). The cytosolic tail of ORF7a contains a dilysine (KRKTE) endoplasmic reticulum (ER) retrieval signal (ERRS) that mediates protein trafficking to the ER-Golgi intermediate compartment (ERGIC) (Nelson et al., 2005).

The Δ115 nt mutation in ORF7a introduces a premature stop codon that eliminates β5, β6, and β7, two of the cystines that form disulfides (Cys58 and Cys67), the TM, and the cytosolic tail (Figures 2A and 2B). This truncation is expected to destabilize the protein structure and significantly impact protein function and trafficking in the host cell. To determine how loss of TM and sorting signal affects protein localization, we cloned and expressed FLAG-tagged wild-type and truncated ORF7a proteins in HEK293T-hACE2 cells. The wild-type ORF7a accumulated in the perinuclear region of the cell, which is consistent with previously reported ERGIC localization (Figure 2D) (Martin-Sancho et al., 2020; Nelson et al., 2005). In contrast, the truncated ORF7a is distributed throughout the cytoplasm and does not associate with specific subcellular compartments, which is consistent with the loss of the TM domain and the ERRS signals required for protein targeting (Figure 2E).

Extent of the truncation and the defect in intracellular targeting suggests possible loss of ORF7a function. Along with several SARS-CoV-2 accessory proteins, ORF7a has been implicated in suppression of host IFN response to the infection (Xia et al., 2020). To test the effect of the truncated ORF7a protein on IFN signaling, we generated reporter HEK293T cells with integrated luciferase reporter gene controlled by the interferon-stimulated response element (ISRE). In these cells, activation of interferon response drives reporter expression, which is quantified using a luciferase assay. To test immune suppression, we overexpressed the wild-type and the deletion mutant of ORF7a (ORF7a$^{\Delta 115}$) from plasmids and the stimulated cells with IFNα2b. The ORF7a WT protein suppressed IFN response by 34% ($p = 0.0074$) compared with cells transfected with control plasmid, which is consistent with recent results by Xia et al. (2020). In contrast, the ORF7a$^{\Delta 115}$ protein failed to suppress IFN response and showed no significant difference to a control (mCherry) plasmid (Figure 2F). These results indicate that the Δ115 mutation in *ORF7a* has a loss-of-function effect that negates antagonism of IFN signaling.

ORF7a mutation has no collateral effect on ORF7b

The ORF7a gene overlaps with the downstream ORF7b gene (Figure S2). To determine if the Δ115 mutation in ORF7a impacts ORF7b, we first examined whether it eliminates a transcription-regulatory sequence (TRS) that is required for subgenomic RNA (sgRNA) synthesis. None of the TRSs identified via direct RNA sequencing (RNA-seq) of SARS-CoV-2 overlap with the Δ115 mutation site (Kim et al., 2020), suggesting that ORF7b transcription is not affected (Figure S2). To confirm this prediction, we used RT-PCR with primers that detect ORF7a and ORF7b sgRNAs (Figure 2G). In this assay, we infected 293T-hACE2 cells (MOI = 0.05) with ORF7a^{WT} or ORF7a$^{\Delta 115}$ viral strains and extracted total RNA from cells at 24 h postinfection (hpi). Both viruses produced specific RT-PCR products corresponding to ORF7a and ORF7b sgRNAs. Finally, to verify that the ORF7a$^{\Delta 115}$ variant does not impact ORF7b translation, we probed cell lysates 24 hpi with an anti-ORF7b antibody (Figure 2H). We detected ORF7b protein in both viral strains with band intensities that suggest similar expression levels. Collectively, these data indicate that the ORF7a$^{\Delta 115}$ mutation has no collateral effect on the adjacent gene.

ORF7a$^{\Delta 115}$ isolate displays a replication defect

To investigate the phenotype of SARS-CoV-2 Δ115 variant, we infected 293T-hACE2 and Vero E6 cells with ORF7a^{WT} and ORF7a$^{\Delta 115}$ viruses at an MOI of 0.05 and measured viral RNA

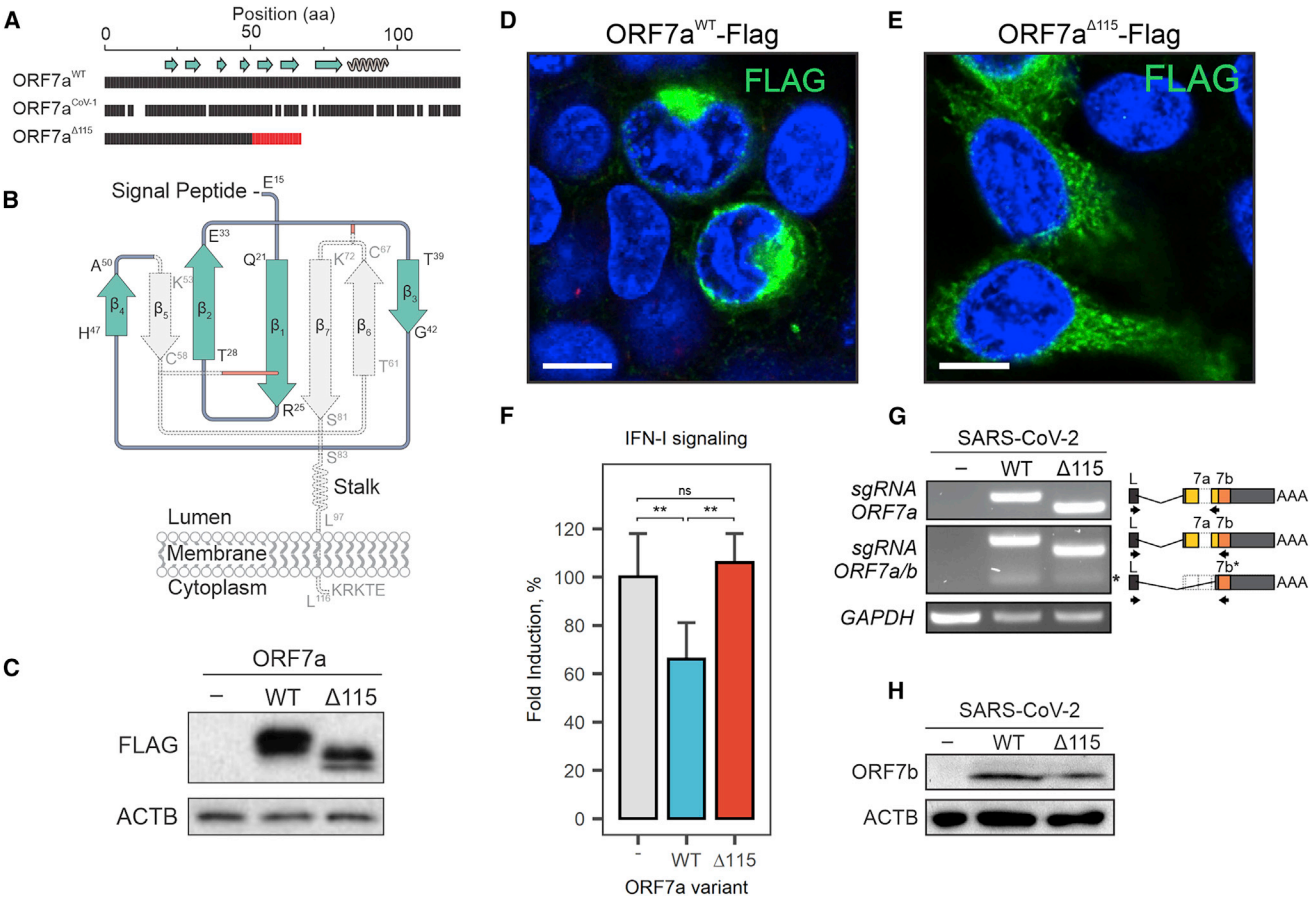

Figure 2. ORF7a truncation results in loss of function

(A) Amino acid (aa) sequence alignment of SARS-CoV-2 ORF7a^{WT}, ORF7a$^{\Delta 115}$, and SARS-CoV-1 ORF7a. Gaps show non-matching positions; red shows 17-aa sequence resulting from a frameshift in the ORF7a mutant. Beta strands (arrows) and alpha helices (coil) are shown above the alignment.

(B) Diagram of SARS-CoV-2 ORF7a Ig-like fold. Disulfide bonds that stabilize the β sandwich structure are shown with red lines. The portion of the protein eliminated by the deletion is shown in gray.

(C) C-terminally FLAG-tagged ORF7a^{WT} and ORF7a$^{\Delta 115}$ were cloned and overexpressed in HEK293T-hACE2. Protein expression was confirmed with western blot using anti-FLAG antibody. β-Actin (ACTB) was used as a loading control.

(D and E) FLAG-tagged ORF7a^{WT} (D) or ORF7a$^{\Delta 115}$ (E) expressed in HEK293T-hACE2 cells. Immunostaining was performed using an anti-FLAG antibody (green). Cell nuclei were stained with Hoechst 33342 (blue). White scale bar is 10 μm.

(F) HEK293T cells with integrated ISRE-luciferase reporter were transfected with pLV-mCherry ("-"), ORF7a^{WT}, or ORF7a$^{\Delta 115}$ plasmids. Transfected cells were treated with 5 ng/mL human recombinant IFN-α2b for 24 h, and induction of type I IFN signaling was measured with luciferase assay. Fold induction versus non-treated control was determined and normalized to mCherry control. Means (n = 6) were compared with one-way ANOVA ($p = 0.00162$). Pairwise comparisons were performed using post hoc Tukey's test. Data are shown as mean ± SD. $^{**}p < 0.01$; $^{ns}p > 0.05$.

(G) ORF7a and ORF7b sgRNAs were identified by RT-PCR. Lower molecular weight band corresponding to ORF7b sgRNA is indicated with asterisk (*). Diagram on the right shows primer (arrows) positions. Specificity of PCR products was confirmed with Sanger sequencing. *GAPDH* was used as a control for cDNA synthesis.

(H) Lysates from SARS-CoV-2-infected cells were probed with antibodies raised against ORF7b protein. ACTB was used as a loading control.

replication using qRT-PCR (Figures 3A and 3B). In this assay, we used viral strains sharing the same haplotype (C241T, C3037T, C14408T, A23403G) that defines the SARS-CoV-2 B.1 lineage and its derivatives (Figure S3A) (Rambaut et al., 2020a). Over the course of 120 h, ORF7a^{WT} viral RNA level increased ~960-fold in supernatants from Vero E6 cells (Figure 3A) and ~270-fold in supernatants from 293T-hACE2 cells (Figure 3B). The ORF7a$^{\Delta 115}$ virus displayed limited replication that resulted in only 18.6-fold and 7-fold RNA level increase at 120 hpi in VeroE6 and 293T-hACE2, respectively. This growth defect reaches statistical significance starting at 6 hpi in Vero E6 cells ($p = 0.0135$) and 24 hpi in 293T-hACE2 cells ($p = 6.2 \times 10^{-5}$).

To determine if this phenotype results from a defect in viral egress only or if viral RNA replication in the host is also affected, we examined early steps in the infection. We extracted total RNA from the infected 293T-hACE2 cells at 0.5, 6, and 24 hpi and measured SARS-CoV-2 RNA with qRT-PCR. Compared with wild type, ORF7a$^{\Delta 115}$ RNA level was reduced 2.1-fold inside the host at 6 hpi ($p = 0.002$) and 4.3-fold at 24 hpi ($p = 0.02$) (Figure 3C). This decrease in viral

CellPress
OPEN ACCESS

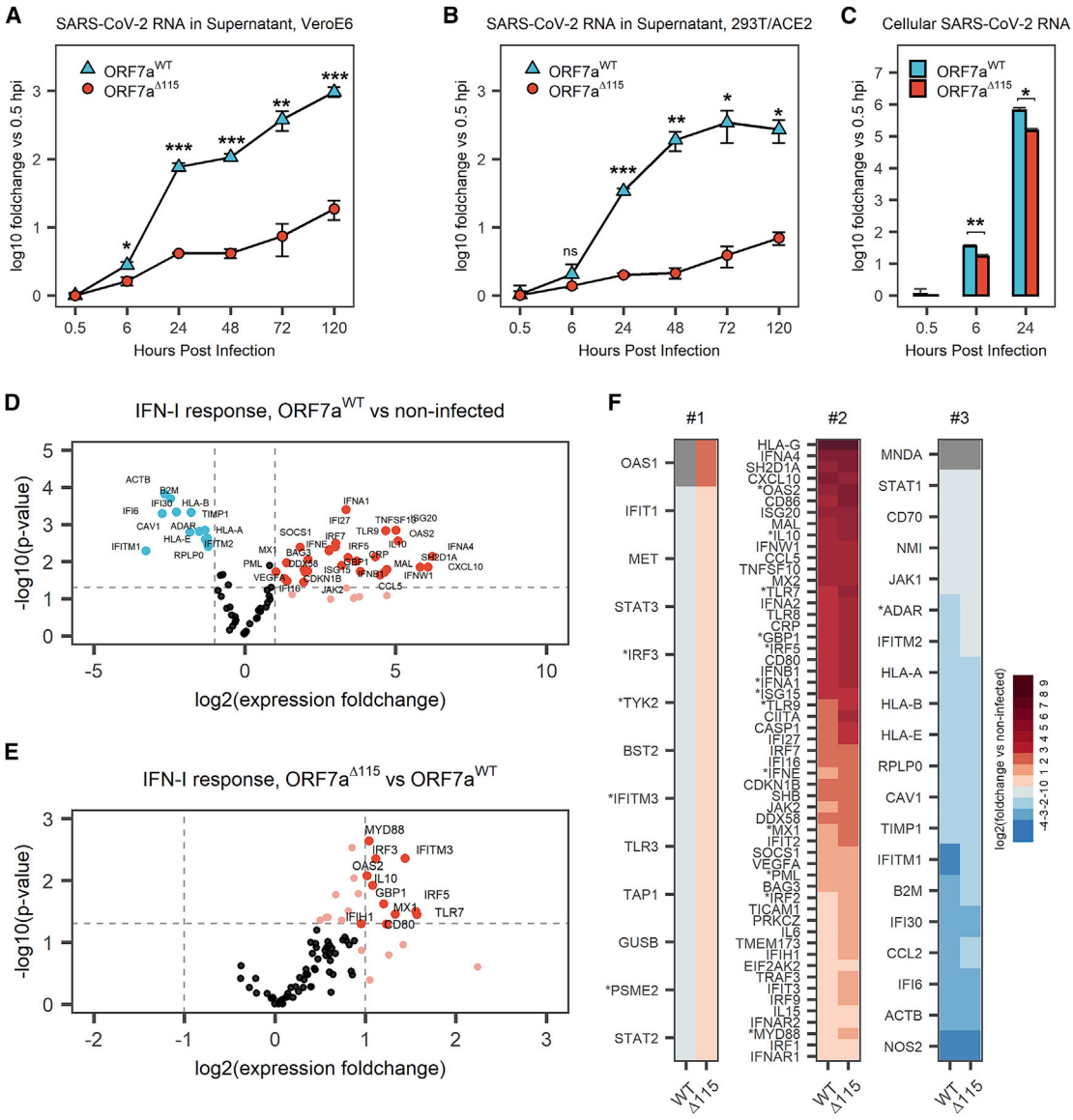

Figure 3. The ORF7a$^{\Delta 115}$ mutation results in replication and immune suppression defects

(A and B) VeroE6 (A) or HEK293T-hACE2 (B) cells were infected with ORF7a^{WT} or ORF7a$^{\Delta 115}$ SARS-CoV-2 strain at MOI = 0.05. Viral RNA was measured in supernatant using qRT-PCR at different time points after infection. Measured RNA levels were normalized (using ΔCt method) to RNA levels at 0.5 hpi.

(C) Total RNA was extracted from infected HEK293T-hACE2 cells, and viral RNA was measured. The ΔΔCt method was used to normalize viral RNA levels to host RNA (*ACTB*) and 0.5 hpi time point. Data in (A)–(C) are presented as mean ± SD of three biological replicates. Significance levels: *$p < 0.05$, **$p < 0.01$, ***$p < 0.001$, or $^{ns}p > 0.05$ (no significant difference).

(D) Volcano plot showing IFN-I response in 293T-hACE2 cells infected with ORF7a^{WT} SARS-CoV-2 strain at MOI = 0.05. Expression of IFN-I response genes was studied 24 hpi using qRT-PCR array targeting 91 human transcripts (88 targets and 3 references). Experiment was performed in three biological replicates. Dashed lines show regulation (≥2-fold) and statistical significance ($p < 0.05$) thresholds. Each dot represents mean (n = 3) normalized expression of a single gene relative to non-infected host. Genes that passed the threshold are labeled.

(E) Volcano plot showing IFN-I response in ORF7a$^{\Delta 115}$ versus ORF7a^{WT} infection.

(F) Data shown in (D) and Figure S3A were plotted as a heatmap. Genes were classified into three groups. Group #1 genes are oppositely regulated between the two viral strains. Group #2 genes are upregulated by both ORF7a^{WT} and ORF7a$^{\Delta 115}$. Group #3 genes are downregulated in both. Genes that have statistically significant difference in expression between two viral strains are marked with asterisk. Gray shows genes with no detectable expression over 40 cycles of qRT-PCR.

RNA in the host cell differs from the corresponding decrease in the supernatant RNA at 24 hpi (4.3-fold versus 16.8-fold, respectively; Figures 3B and 3C). This disparity suggests that observed growth defect in the SARS-CoV-2 Δ115 variant might result from defects in genomic RNA replication and transcription, as well as in viral egress.

ORF7a$^{\Delta 115}$ virus induces elevated IFN-I response *in vitro*

Suppressed or delayed IFN responses characterize SARS-CoV-2 infections (Lei et al., 2020). The C-terminal truncation of ORF7a limits suppression of the type I IFN signaling (Figure 2F). Therefore, we hypothesized that ORF7a$^{\Delta 115}$ virus isolated from the community is deficient in antagonizing IFN response.

To test this hypothesis, we measured expression of type I IFN response genes upon infection with ORF7a^{WT} and ORF7a$^{\Delta 115}$ strains using a qRT-PCR array targeting 91 human transcripts (Table S2). The array included three reference genes that we used to normalize expression of 88 target genes. In agreement with recent transcriptomic studies, we detected a type I IFN-mediated antiviral response after infecting HEK293T-hACE2 with SARS-CoV-2 isolates (Figure 3D; Figure S3B) (Banerjee et al., 2020; Blanco-Melo et al., 2020). Out of 88 type I IFN response genes included in the qRT-PCR array, 42 were differentially expressed ($\geq$2-fold change, $p < 0.05$) in ORF7a^{WT}-infected cells and 55 in ORF7a$^{\Delta 115}$ infection, as compared with the non-infected control (Figure 3D; Figure S3B). Both viruses stimulated expression of multiple type I interferon genes, antiviral ISGs, ILs, and proinflammatory cytokines (Table S2).

To understand the effect of ORF7a$^{\Delta 115}$ on the host type I IFN response, we compared expression of genes targeted with qRT-PCR array between the two viruses. In general, the ORF7a$^{\Delta}$115 variant induces elevated type I IFN response to the infection (Figures S3C and S3D). The median expression fold change of 88 genes targeted in the qRT-PCR array was 1.72 in ORF7a^{WT} and 2.51 in ORF7a$^{\Delta 115}$ virus ($p = 1.4E-12$; Figure S3C). Analysis of genes differentially expressed between the two viral infections results in an asymmetric volcano plot (Figure 3E). A subset of ISGs had expression levels that are significantly different ($p < 0.05$) between the two viral infections (Figures 3E and 3F; Table S2). This subset includes sensors (*TLR7*), signal transducers (*MYD88, OAS2*), transcriptional regulators (*IRF3*, *IRF5*), and restriction factors (*GBP1*, *IFITM3*, *MX1*) known to combat infections by RNA viruses (Schoggins, 2019). One of these differentially expressed ISGs (*IFITM3*) restricts SARS-CoV-2 entry (Shi et al., 2021; Zang et al., 2020). Additionally, polymorphisms in *IFITM3*, *MX1*, and *TLR7* are linked to the severity of COVID-19 (Andolfo et al., 2020; Zhang et al., 2020a; Pati et al., 2021). Upregulation of ISGs indicates that the ORF7a$^{\Delta 115}$ virus is inept at antagonizing the IFN-I response to the infection, which is consistent with results from our ISRE reporter assay (Figure 2F).

DISCUSSION

In this study, we use genomic surveillance and phylogenetics to identify ORF7a variants that have emerged globally throughout the SARS-CoV-2 pandemic. Local occurrence of ORF7a mutations has been reported by others (Addetia et al., 2020; Holland et al., 2020; Rosenthal et al., 2020). However, the effect of these mutations on viral fitness and host immune responses has not been investigated. Here, we isolated a virus with a deletion mutation in ORF7a (ORF7a$^{\Delta 115}$) and show that this genotype results in an *in vitro* growth defect. This growth defect is associated with elevated IFN response to SARS-CoV-2.

Interferon systems are a frontline of host defense that signals infection and elicits an antiviral state (McNab et al., 2015). Pretreatment with type I, type II, and type III IFNs restricts SARS-CoV-2 infection and replication in cell culture (Mantlo et al., 2020; Miorin et al., 2020). SARS-CoV-2 deploys multiple proteins (e.g., nsp6, nsp13, ORF6, ORF7a, ORF7b, and ORF9b) to shut down IFN signaling and dampen innate immune responses (Jiang et al., 2020; Lei et al., 2020; Xia et al., 2020), in particular, when overexpressed ORF7a subverts STAT2 phosphorylation, blocking IFN-dependent transcriptional activation of antiviral ISGs (Xia et al., 2020). Both type I and III IFNs signal through the JAK-STAT pathway and overlap substantially in the transcriptional responses they induce (Kotenko and Durbin, 2017). Therefore, ORF7a likely suppresses both IFN types; however, its role in suppressing the type III IFN response has yet to be verified (Xia et al., 2020). Using the ISRE reporter system, we show that C-terminal truncation negates the ability of ORF7a to suppress IFN signaling (Figure 2). The ORF7a$^{\Delta 115}$ variant shows limited replication in HEK293T-hACE2, as well as in Vero E6, the latter of which does not express type I IFN genes (Emeny and Morgan, 1979; Osada et al., 2014). Although type I IFN genes are deleted in Vero E6 cells, the type III IFNs are intact and are activated upon infection with RNA viruses, which results in ISG upregulation (Stoltz and Klingström, 2010; Wang et al., 2020). ISGs exert anti-viral activities that combat the infection (Schoggins, 2019). We hypothesize that the replication defect of the ORF7a$^{\Delta 115}$ strain in Vero E6 and 293T-hACE2 cells results from an IFN-dependent response that the virus fails to suppress.

Several groups have replaced ORF7a with a reporter gene (Hou et al., 2020; Thi Nhu Thao et al., 2020; Xie et al., 2020). Thi Nhu Thao et al. (2020) show that complete deletion of ORF7a reduces replication of the synthetic virus, which agrees well with growth defect in the ORF7a$^{\Delta 115}$ strain. However, two other studies have not observed this effect. We believe that our results with a naturally occurring ORF7a deletion provide valuable insight to this discussion. Finally, it should be noted that different mutations (i.e., complete deletion versus partial) might have a different outcome for the viral phenotype.

Cytokine profiling and RNA-seq of clinical samples reveal suppressed or delayed IFN responses in COVID-19 patients (Arunachalam et al., 2020; Hadjadj et al., 2020; Lucas et al., 2020). Dysregulated immune responses coupled with exacerbated inflammatory cytokines drive pathogenesis of the disease and correlate with its severity (Zhang et al., 2020b; Tay et al., 2020; Zhou et al., 2020). Here, we detected enhanced IFN signaling in cells infected with a naturally occurring ORF7a$^{\Delta 115}$ variant of SARS-CoV-2.

Given the importance of the IFN response in COVID-19, we anticipate that ORF7a mutations might affect SARS-CoV-2 pathogenicity. Clinical comparisons will be required to examine this potential effect on COVID-19 features.

Deletions in ORF7a, ORF7b, and ORF8 have previously been reported (Addetia et al., 2020; Holland et al., 2020; Rosenthal et al., 2020; Su et al., 2020). Similar deletions emerged in Middle East Respiratory Syndrome (MERS)- and SARS-CoV, which were linked to viral attenuation (Chinese SARS Molecular Epidemiology Consortium, 2004; Muth et al., 2018). A 382-nt deletion in ORF8 is associated with milder SARS-CoV-2 infection in patients (Young et al., 2020). Although this mutation affects clinical

features of COVID-19, it has no evident effect on viral replication or host transcriptional responses in human cell culture (Gamage et al., 2020).

Several studies illustrate how persistent SARS-CoV-2 infections in immunocompromised hosts associate with accelerated viral evolution (Avanzato et al., 2020; Choi et al., 2020). In these hosts there is less selective pressure on viral anti-immune proteins, which might permit loss-of-function mutations in accessory genes. The ORF7a$^{\Delta 115}$ variant that we isolated was present in only seven genomes over a course of ~1.5 months in a local community and then disappeared. We hypothesize that deletions in accessory genes, such as ORF7a$^{\Delta 115}$, might emerge in immunocompromised patients but do not persist in the immunocompetent population. Similarly, a deletion mutation in ORF8 (i.e., Δ382), which was associated with milder COVID-19 disease, disappeared soon after it was discovered (Young et al., 2020). However, founder effect or mutations that co-occur with other mutations that increase transmissibility (e.g., spike mutations) can result in fixation of an otherwise attenuating mutation. A new more transmissible lineage of SARS-CoV-2 (i.e., B.1.1.7) has recently emerged (Davies et al., 2021; Rambaut et al., 2020b). Aside from changes in the Spike protein, this lineage also includes a premature stop codon in the accessory ORF8 that truncates most of the protein (Volz et al., 2021). This lineage might illustrate the second scenario for fixing mutations in accessory genes.

Limitations of study

The viral replication defect and cellular immune response assay presented here were performed using HEK293T-hACE2 and Vero E6 cells that are not the natural targets of SARS-CoV-2. However, both cell lines are permissive for SARS-CoV-2 infection and are used extensively to study efficacy of antiviral compounds (Riva et al., 2020), virion assembly (Klein et al., 2020), SARS-CoV-2 entry (Hoffmann et al., 2020), replication (Thi Nhu Thao et al., 2020), and anti-immune activities of SARS-CoV-2 proteins (Xia et al., 2020). Although we acknowledge that our conclusions are limited to Vero E6 and 293T-hACE2 cells, we anticipate that the results presented here will provide important context for clinical comparisons, similar to those recently published for ORF8 (Young et al., 2020).

Studies of naturally occurring SARS-CoV-2 variants have limitations, including unavailability of isogenic controls. Here, we compared two viral isolates, ORF7a^{WT} and ORF7a$^{\Delta 115}$, that in addition to Δ115 differ at several other nucleotide positions (Figure S3A). Although ISRE reporter assay unambiguously links the immunosuppression defect to the truncation of ORF7a, it is not possible to rule out a role for these mutations on the viral life cycle.

STAR★METHODS

Detailed methods are provided in the online version of this paper and include the following:

- KEY RESOURCES TABLE
- RESOURCE AVAILABILITY
  - Lead contact
  - Materials availability
  - Data and code availability
- EXPERIMENTAL MODEL AND SUBJECT DETAILS
  - Cell cultures
  - Plasmids
  - Antibodies
  - Human clinical sample collection and preparation
  - Production and titration of coronavirus stocks
  - Symptom onset data and clinical test results
- METHOD DETAILS
  - Quantitative reverse transcription PCR (qRT-PCR)
  - RT-PCR and SARS-CoV-2 genome sequencing
  - SARS-CoV-2 genome assembly
  - RT-PCR and Sanger sequencing
  - Phylogenetic and ORF7a mutational analysis
  - Western blot
  - Immunocytochemistry
  - IFN inhibition assay
  - SARS-CoV-2 replication assays
  - Type I interferon response assay
- QUANTIFICATION AND STATISTICAL ANALYSIS

SUPPLEMENTAL INFORMATION

Supplemental information can be found online at https://doi.org/10.1016/j.celrep.2021.109197.

ACKNOWLEDGMENTS

We are grateful to members of Bozeman Health that provided de-identified patient samples, specifically C. Nero, D. Smoot, W. Wallace, C. Faurot-Daniels, V. Lawrence, and M. Blauvelt. We are also grateful to M. Flenniken, K. Daughenbaugh, and other members of the COVID task force at MSU for assistance establishing the COVID testing center. We thank the Lefcort lab for generous use of their fluorescent confocal microscope and Dr. Pincus for providing the HEK 293T-hACE2 cells. Research in the Wiedenheft lab is supported by the National Institutes of Health (1R35GM134867), the Montana State University Agricultural Experimental Station, the MJ Murdock Charitable Trust, the Gianforte Foundation, and the MSU Office of the Vice President for Research. We thank the GISAID's EpiFlu Database and contributing laboratories (Table S4). The phylogenetic analysis in this paper would not have been possible without their willingness to share data. The graphical abstract was created with BioRender.

AUTHOR CONTRIBUTIONS

Conceptualization, B.W., A. Nemudryi, and A. Nemudraia; methodology, B.W., A. Nemudraia, A. Nemudryi, D.T.S., and J.F.H.; sample acquisition, D.B. and B.W.; investigation & data collection, A. Nemudraia, A. Nemudryi, D.T.S., J.F.H., J.N., H.L., and K.K.V.; genomics and bioinformatics analysis, T.W., A. Nemudryi, and C.C.; writing – original draft, B.W., A. Nemudryi, A. Nemudraia, and T.W.; writing – review & editing, B.W., A. Nemudryi, A. Nemudraia, T.W., and M.A.J.

DECLARATION OF INTERESTS

B.W. is the founder of SurGene LLC and VIRIS Detection Systems Inc. B.W., A. Nemudryi, and A. Nemudraia are inventors on patents related to CRISPR-Cas systems and applications thereof.

Received: February 3, 2021
Revised: April 4, 2021
Accepted: May 10, 2021
Published: June 1, 2021

REFERENCES

Addetia, A., Xie, H., Roychoudhury, P., Shrestha, L., Loprieno, M., Huang, M.-L., Jerome, K.R., and Greninger, A.L. (2020). Identification of multiple large deletions in ORF7a resulting in in-frame gene fusions in clinical SARS-CoV-2 isolates. J. Clin. Virol. *129*, 104523.

Andersen, K.G., Rambaut, A., Lipkin, W.I., Holmes, E.C., and Garry, R.F. (2020). The proximal origin of SARS-CoV-2. Nat. Med. *26*, 450–452.

Andolfo, I., Russo, R., Lasorsa, A.V., Cantalupo, S., Rosato, B.E., Bonfiglio, F., Frisso, G., Pasquale, A., Cassese, G.M., Servillo, G., et al. (2020). Common variants at 21q22.3 locus influence MX1 gene expression and susceptibility to severe COVID-19. medRxiv. https://doi.org/10.1101/2020.12.18.20248470.

Arunachalam, P.S., Wimmers, F., Mok, C.K.P., Perera, R.A.P.M., Scott, M., Hagan, T., Sigal, N., Feng, Y., Bristow, L., Tak-Yin Tsang, O., et al. (2020). Systems biological assessment of immunity to mild versus severe COVID-19 infection in humans. Science *369*, 1210–1220.

Avanzato, V.A., Matson, M.J., Seifert, S.N., Pryce, R., Williamson, B.N., Anzick, S.L., Barbian, K., Judson, S.D., Fischer, E.R., Martens, C., et al. (2020). Case Study: Prolonged Infectious SARS-CoV-2 Shedding from an Asymptomatic Immunocompromised Individual with Cancer. Cell *183*, 1901–1912.e9.

Banerjee, A., El-Sayes, N., Budylowski, P., Richard, D., Maan, H., Aguiar, J.A., Baid, K., D'Agostino, M.R., Ang, J.C., Tremblay, B.J.M., et al. (2020). Experimental and natural evidence of SARS-CoV-2 infection-induced activation of type I interferon responses. bioRxiv. https://doi.org/10.1101/2020.06.18.158154.

Bedford, T., Greninger, A.L., Roychoudhury, P., Starita, L.M., Famulare, M., Huang, M.-L., Nalla, A., Pepper, G., Reinhardt, A., Xie, H., et al.; Seattle Flu Study Investigators (2020). Cryptic transmission of SARS-CoV-2 in Washington state. Science *370*, 571–575.

Blanco-Melo, D., Nilsson-Payant, B.E., Liu, W.-C., Uhl, S., Hoagland, D., Møller, R., Jordan, T.X., Oishi, K., Panis, M., Sachs, D., et al. (2020). Imbalanced Host Response to SARS-CoV-2 Drives Development of COVID-19. Cell *181*, 1036–1045.e9.

Chinese SARS Molecular Epidemiology Consortium (2004). Molecular evolution of the SARS coronavirus during the course of the SARS epidemic in China. Science *303*, 1666–1669.

Choi, B., Choudhary, M.C., Regan, J., Sparks, J.A., Padera, R.F., Qiu, X., Solomon, I.H., Kuo, H.-H., Boucau, J., Bowman, K., et al. (2020). Persistence and Evolution of SARS-CoV-2 in an Immunocompromised Host. N. Engl. J. Med. *383*, 2291–2293.

Davies, N.G., Abbott, S., Barnard, R.C., Jarvis, C.I., Kucharski, A.J., Munday, J.D., Pearson, C.A.B., Russell, T.W., Tully, D.C., Washburne, A.D., et al.; CMMID COVID-19 Working Group; COVID-19 Genomics UK (COG-UK) Consortium (2021). Estimated transmissibility and impact of SARS-CoV-2 lineage B.1.1.7 in England. Science *372*, eabg3055.

Emeny, J.M., and Morgan, M.J. (1979). Regulation of the interferon system: evidence that Vero cells have a genetic defect in interferon production. J. Gen. Virol. *43*, 247–252.

Gamage, A.M., Tan, K.S., Chan, W.O.Y., Liu, J., Tan, C.W., Ong, Y.K., Thong, M., Andiappan, A.K., Anderson, D.E., Wang, Y., and Wang, L.F. (2020). Infection of human Nasal Epithelial Cells with SARS-CoV-2 and a 382-nt deletion isolate lacking ORF8 reveals similar viral kinetics and host transcriptional profiles. PLoS Pathog. *16*, e1009130.

Grubaugh, N.D., Gangavarapu, K., Quick, J., Matteson, N.L., De Jesus, J.G., Main, B.J., Tan, A.L., Paul, L.M., Brackney, D.E., Grewal, S., et al. (2019). An amplicon-based sequencing framework for accurately measuring intrahost virus diversity using PrimalSeq and iVar. Genome Biol *20*, 8.

Hachim, A., Kavian, N., Cohen, C.A., Chin, A.W.H., Chu, D.K.W., Mok, C.K.P., Tsang, O.T.Y., Yeung, Y.C., Perera, R.A.P.M., Poon, L.L.M., et al. (2020). ORF8 and ORF3b antibodies are accurate serological markers of early and late SARS-CoV-2 infection. Nat. Immunol. *21*, 1293–1301.

Hadjadj, J., Yatim, N., Barnabei, L., Corneau, A., Boussier, J., Smith, N., Péré, H., Charbit, B., Bondet, V., Chenevier-Gobeaux, C., et al. (2020). Impaired type I interferon activity and inflammatory responses in severe COVID-19 patients. Science *369*, 718–724.

Harcourt, J., Tamin, A., Lu, X., Kamili, S., Sakthivel, S.K., Murray, J., Queen, K., Tao, Y., Paden, C.R., Zhang, J., et al. (2020). Severe Acute Respiratory Syndrome Coronavirus 2 from Patient with Coronavirus Disease, United States. Emerg. Infect. Dis. *26*, 1266–1273.

Hoffmann, M., Kleine-Weber, H., Schroeder, S., Krüger, N., Herrler, T., Erichsen, S., Schiergens, T.S., Herrler, G., Wu, N.H., Nitsche, A., et al. (2020). SARS-CoV-2 Cell Entry Depends on ACE2 and TMPRSS2 and Is Blocked by a Clinically Proven Protease Inhibitor. Cell *181*, 271–280.e8.

Holland, L.A., Kaelin, E.A., Maqsood, R., Estifanos, B., Wu, L.I., Varsani, A., Halden, R.U., Hogue, B.G., Scotch, M., and Lim, E.S. (2020). An 81-Nucleotide Deletion in SARS-CoV-2 ORF7a Identified from Sentinel Surveillance in Arizona (January to March 2020). J. Virol. *94*, e00711-20.

Holshue, M.L., DeBolt, C., Lindquist, S., Lofy, K.H., Wiesman, J., Bruce, H., Spitters, C., Ericson, K., Wilkerson, S., Tural, A., et al.; Washington State 2019-nCoV Case Investigation Team (2020). First Case of 2019 Novel Coronavirus in the United States. N. Engl. J. Med. *382*, 929–936.

Hou, Y.J., Okuda, K., Edwards, C.E., Martinez, D.R., Asakura, T., Dinnon, K.H., 3rd, Kato, T., Lee, R.E., Yount, B.L., Mascenik, T.M., et al. (2020). SARS-CoV-2 Reverse Genetics Reveals a Variable Infection Gradient in the Respiratory Tract. Cell *182*, 429–446.e14.

Jiang, H.W., Zhang, H.N., Meng, Q.F., Xie, J., Li, Y., Chen, H., Zheng, Y.X., Wang, X.N., Qi, H., Zhang, J., et al. (2020). SARS-CoV-2 Orf9b suppresses type I interferon responses by targeting TOM70. Cell. Mol. Immunol. *17*, 998–1000.

Kim, D., Lee, J.-Y., Yang, J.-S., Kim, J.W., Kim, V.N., and Chang, H. (2020). The Architecture of SARS-CoV-2 Transcriptome. Cell *181*, 914–921.e10.

Klein, S., Cortese, M., Winter, S.L., Wachsmuth-Melm, M., Neufeldt, C.J., Cerikan, B., Stanifer, M.L., Boulant, S., Bartenschlager, R., and Chlanda, P. (2020). SARS-CoV-2 structure and replication characterized by in situ cryo-electron tomography. bioRxiv. https://doi.org/10.1101/2020.06.23.167064.

Konno, Y., Kimura, I., Uriu, K., Fukushi, M., Irie, T., Koyanagi, Y., Sauter, D., Gifford, R.J., Nakagawa, S., and Sato, K.; USFQ-COVID19 Consortium (2020). SARS-CoV-2 ORF3b Is a Potent Interferon Antagonist Whose Activity Is Increased by a Naturally Occurring Elongation Variant. Cell Rep. *32*, 108185.

Korber, B., Fischer, W.M., Gnanakaran, S., Yoon, H., Theiler, J., Abfalterer, W., Hengartner, N., Giorgi, E.E., Bhattacharya, T., Foley, B., et al.; Sheffield COVID-19 Genomics Group (2020). Tracking Changes in SARS-CoV-2 Spike: Evidence that D614G Increases Infectivity of the COVID-19 Virus. Cell *182*, 812–827.e19.

Kotenko, S.V., and Durbin, J.E. (2017). Contribution of type III interferons to antiviral immunity: location, location, location. J. Biol. Chem. *292*, 7295–7303.

Lei, X., Dong, X., Ma, R., Wang, W., Xiao, X., Tian, Z., Wang, C., Wang, Y., Li, L., Ren, L., et al. (2020). Activation and evasion of type I interferon responses by SARS-CoV-2. Nat. Commun. *11*, 3810.

Lemieux, J.E., Siddle, K.J., Shaw, B.M., Loreth, C., Schaffner, S.F., Gladden-Young, A., Adams, G., Fink, T., Tomkins-Tinch, C.H., Krasilnikova, L.A., et al. (2021). Phylogenetic analysis of SARS-CoV-2 in Boston highlights the impact of superspreading events. Science *371*, eabe3261.

Li, H. (2018). Minimap2: pairwise alignment for nucleotide sequences. Bioinformatics *34*, 3094–3100.

Loveday, E.K., Hain, K.S., Kochetkova, I., Hedges, J.F., Robison, A., Snyder, D.T., Brumfield, S.K., Young, M.J., Jutila, M.A., Chang, C.B., and Taylor, M.P. (2021). Effect of Inactivation Methods on SARS-CoV-2 Virion Protein and Structure. Viruses *13*, 562.

Lucas, C., Wong, P., Klein, J., Castro, T.B.R., Silva, J., Sundaram, M., Ellingson, M.K., Mao, T., Oh, J.E., Israelow, B., et al.; Yale IMPACT Team (2020). Longitudinal analyses reveal immunological misfiring in severe COVID-19. Nature *584*, 463–469.

Mantlo, E., Bukreyeva, N., Maruyama, J., Paessler, S., and Huang, C. (2020). Antiviral activities of type I interferons to SARS-CoV-2 infection. Antiviral Res. *179*, 104811.

Martin-Sancho, L., Lewinski, M.K., Pache, L., Stoneham, C.A., Yin, X., Pratt, D., Churas, C., Rosenthal, S.B., Liu, S., De Jesus, P.D., et al. (2020). Functional Landscape of SARS-CoV-2 Cellular Restriction. bioRxiv. https://doi.org/10.1101/2020.09.29.319566.

McNab, F., Mayer-Barber, K., Sher, A., Wack, A., and O'Garra, A. (2015). Type I interferons in infectious disease. Nat. Rev. Immunol. *15*, 87–103.

Miorin, L., Kehrer, T., Sanchez-Aparicio, M.T., Zhang, K., Cohen, P., Patel, R.S., Cupic, A., Makio, T., Mei, M., Moreno, E., et al. (2020). SARS-CoV-2 Orf6 hijacks Nup98 to block STAT nuclear import and antagonize interferon signaling. Proc. Natl. Acad. Sci. USA *117*, 28344–28354.

Muth, D., Corman, V.M., Roth, H., Binger, T., Dijkman, R., Gottula, L.T., Gloza-Rausch, F., Balboni, A., Battilani, M., Rihtarič, D., et al. (2018). Attenuation of replication by a 29 nucleotide deletion in SARS-coronavirus acquired during the early stages of human-to-human transmission. Sci. Rep. *8*, 15177.

Nelson, C.A., Pekosz, A., Lee, C.A., Diamond, M.S., and Fremont, D.H. (2005). Structure and intracellular targeting of the SARS-coronavirus Orf7a accessory protein. Structure *13*, 75–85.

Osada, N., Kohara, A., Yamaji, T., Hirayama, N., Kasai, F., Sekizuka, T., Kuroda, M., and Hanada, K. (2014). The genome landscape of the african green monkey kidney-derived vero cell line. DNA Res. *21*, 673–683.

Pati, A., Padhi, S., Suvankar, S., and Panda, A.K. (2021). Minor Allele of Interferon-Induced Transmembrane Protein 3 Polymorphism (rs12252) Is Covered Against Severe Acute Respiratory Syndrome Coronavirus 2 Infection and Mortality: A Worldwide Epidemiological Investigation. J. Infect. Dis. *223*, 175–178.

Quick, J., Grubaugh, N.D., Pullan, S.T., Claro, I.M., Smith, A.D., Gangavarapu, K., Oliveira, G., Robles-Sikisaka, R., Rogers, T.F., Beutler, N.A., et al. (2017). Multiplex PCR method for MinION and Illumina sequencing of Zika and other virus genomes directly from clinical samples. Nat. Protoc. *12*, 1261–1276.

Rambaut, A., Holmes, E.C., O'Toole, Á., Hill, V., McCrone, J.T., Ruis, C., du Plessis, L., and Pybus, O.G. (2020a). A dynamic nomenclature proposal for SARS-CoV-2 lineages to assist genomic epidemiology. Nat. Microbiol. *5*, 1403–1407.

Rambaut, A., Loman, N., Pybus, O., Barclay, W., Barrett, J., Carabelli, A., Connor, T., Peacock, T., Robertson, D.L., and Volz, E.; on behalf of COVID-19 Genomics Consortium UK (CoG-UK) (2020b). Preliminary genomic characterisation of an emergent SARS-CoV-2 lineage in the UK defined by a novel set of spike mutations. https://virological.org/t/563.

Riva, L., Yuan, S., Yin, X., Martin-Sancho, L., Matsunaga, N., Pache, L., Burgstaller-Muehlbacher, S., De Jesus, P.D., Teriete, P., Hull, M.V., et al. (2020). Discovery of SARS-CoV-2 antiviral drugs through large-scale compound repurposing. Nature *586*, 113–119.

Rosenthal, S.H., Kagan, R.M., Gerasimova, A., Anderson, B., Grover, D., Hua, M., Liu, Y., Owen, R., and Lacbawan, F. (2020). Identification of eight SARS-CoV-2 ORF7a deletion variants in 2,726 clinical specimens. bioRxiv. https://doi.org/10.1101/2020.12.10.418855.

Schoggins, J.W. (2019). Interferon-Stimulated Genes: What Do They All Do? Annu. Rev. Virol. *6*, 567–584.

Shi, G., Kenney, A.D., Kudryashova, E., Zani, A., Zhang, L., Lai, K.K., Hall--Stoodley, L., Robinson, R.T., Kudryashov, D.S., Compton, A.A., and Yount, J.S. (2021). Opposing activities of IFITM proteins in SARS-CoV-2 infection. EMBO J. *40*, e106501.

Stoltz, M., and Klingström, J. (2010). α/β interferon (IFN-α/β)-independent induction of IFN-λ1 (interleukin-29) in response to Hantaan virus infection. J. Virol. *84*, 9140–9148.

Su, Y.C.F., Anderson, D.E., Young, B.E., Linster, M., Zhu, F., Jayakumar, J., Zhuang, Y., Kalimuddin, S., Low, J.G.H., Tan, C.W., et al. (2020). Discovery and Genomic Characterization of a 382-Nucleotide Deletion in ORF7b and ORF8 during the Early Evolution of SARS-CoV-2. MBio *11*, e01610-20.

Tan, Y., Schneider, T., Leong, M., Aravind, L., and Zhang, D. (2020). Novel Immunoglobulin Domain Proteins Provide Insights into Evolution and Pathogenesis of SARS-CoV-2-Related Viruses. MBio *11*, e00760-20.

Tay, M.Z., Poh, C.M., Rénia, L., MacAry, P.A., and Ng, L.F.P. (2020). The trinity of COVID-19: immunity, inflammation and intervention. Nat. Rev. Immunol. *20*, 363–374.

Thi Nhu Thao, T., Labroussaa, F., Ebert, N., V'kovski, P., Stalder, H., Portmann, J., Kelly, J., Steiner, S., Holwerda, M., Kratzel, A., et al. (2020). Rapid reconstruction of SARS-CoV-2 using a synthetic genomics platform. Nature *582*, 561–565.

Tyson, J.R., James, P., Stoddart, D., Sparks, N., Wickenhagen, A., Hall, G., Choi, J.H., Lapointe, H., Kamelian, K., Smith, A.D., et al. (2020). Improvements to the ARTIC multiplex PCR method for SARS-CoV-2 genome sequencing using nanopore. bioRxiv. https://doi.org/10.1101/2020.09.04.283077.

van Dorp, L., Richard, D., Tan, C.C.S., Shaw, L.P., Acman, M., and Balloux, F. (2020). No evidence for increased transmissibility from recurrent mutations in SARS-CoV-2. Nat. Commun. *11*, 5986.

Volz, E., Mishra, S., Chand, M., Barrett, J.C., Johnson, R., Geidelberg, L., Hinsley, W.R., Laydon, D.J., Dabrera, G., O'Toole, Á., et al. (2021). Transmission of SARS-CoV-2 Lineage B.1.1.7 in England: Insights from linking epidemiological and genetic data. medRxiv. https://doi.org/10.1101/2020.12.30.20249034.

Wang, C., Shan, L., Qu, S., Xue, M., Wang, K., Fu, F., Wang, L., Wang, Z., Feng, L., Xu, W., and Liu, P. (2020). The Coronavirus PEDV Evades Type III Interferon Response Through the miR-30c-5p/SOCS1 Axis. Front. Microbiol. *11*, 1180.

Wu, F., Zhao, S., Yu, B., Chen, Y.M., Wang, W., Song, Z.G., Hu, Y., Tao, Z.W., Tian, J.H., Pei, Y.Y., et al. (2020). A new coronavirus associated with human respiratory disease in China. Nature *579*, 265–269.

Xia, H., Cao, Z., Xie, X., Zhang, X., Chen, J.Y.-C., Wang, H., Menachery, V.D., Rajsbaum, R., and Shi, P.-Y. (2020). Evasion of Type I Interferon by SARS-CoV-2. Cell Rep. *33*, 108234.

Xie, X., Muruato, A., Lokugamage, K.G., Narayanan, K., Zhang, X., Zou, J., Liu, J., Schindewolf, C., Bopp, N.E., Aguilar, P.V., et al. (2020). An Infectious cDNA Clone of SARS-CoV-2. Cell Host Microbe *27*, 841–848.e3.

Young, B.E., Fong, S.-W., Chan, Y.-H., Mak, T.-M., Ang, L.W., Anderson, D.E., Lee, C.Y.-P., Amrun, S.N., Lee, B., Goh, Y.S., et al. (2020). Effects of a major deletion in the SARS-CoV-2 genome on the severity of infection and the inflammatory response: an observational cohort study. Lancet *396*, 603–611.

Zang, R., Case, J.B., Yutuc, E., Ma, X., Shen, S., Gomez Castro, M.F., Liu, Z., Zeng, Q., Zhao, H., Son, J., et al. (2020). Cholesterol 25-hydroxylase suppresses SARS-CoV-2 replication by blocking membrane fusion. Proc. Natl. Acad. Sci. USA *117*, 32105–32113.

Zhang, Y., Zhang, J., Chen, Y., Luo, B., Yuan, Y., Huang, F., Yang, T., Yu, F., Liu, J., Liu, B., et al. (2020). The ORF8 Protein of SARS-CoV-2 Mediates Immune Evasion through Potently Downregulating MHC-I. bioRxiv. https://doi.org/10.1101/2020.05.24.111823.

Zhang, Y., Qin, L., Zhao, Y., Zhang, P., Xu, B., Li, K., Liang, L., Zhang, C., Dai, Y., Feng, Y., et al. (2020a). Interferon-Induced Transmembrane Protein 3 Genetic Variant rs12252-C Associated With Disease Severity in Coronavirus Disease 2019. J. Infect. Dis. *222*, 34–37.

Zhang, B., Zhou, X., Qiu, Y., Song, Y., Feng, F., Feng, J., Song, Q., Jia, Q., and Wang, J. (2020b). Clinical characteristics of 82 cases of death from COVID-19. PLoS ONE *15*, e0235458.

Zhou, F., Yu, T., Du, R., Fan, G., Liu, Y., Liu, Z., Xiang, J., Wang, Y., Song, B., Gu, X., et al. (2020). Clinical course and risk factors for mortality of adult inpatients with COVID-19 in Wuhan, China: a retrospective cohort study. Lancet *395*, 1054–1062.

Zhou, Z., Huang, C., Zhou, Z., Huang, Z., Su, L., Kang, S., Chen, X., Chen, Q., He, S., Rong, X., et al. (2021). Structural Insight Reveals SARS-CoV-2 ORF7a as an Immunomodulating Factor for Human CD14+ Monocytes. iScience *24*, 102187.

STAR★METHODS

KEY RESOURCES TABLE

REAGENT or RESOURCE	SOURCE	IDENTIFIER
Biological samples		
Nasopharyngeal swabs	Bozeman Health Deaconess Hospital, MT, USA	N/A
Bacterial and virus strains		
SARS-CoV-2 Isolate USA-WA1/2020	BEI Resources	NR-52281
Experimental models: cell lines		
HEK293T-hACE2 cells	BEI Resources	NR-52511
Vero E6	ATCC	Cat#CRL-1586
Recombinant DNA		
pEGFP-N1	Clontech	6085-1
pLV-mCherry	Addgene	36084
pORF7a-CoV2	This study	N/A
pORF7a Δ115-Cov2	This study	N/A
pGreenFire1-ISRE	SBI	TR016PA-1
Antibodies		
Rabbit anti-ACTB	ABclonal	Cat. AC026, RRID:AB_2768234
Mouse anti-FLAG	ThermoFisher Scientific	Cat: MA1-91878-1MG, RRID:AB_2537619
Sheep anti-ORF7b	MRC I PPU, College of Life Sciences, University of Dundee	N/A
Goat anti-mouse IgG peroxidase-conjugated	Jackson ImmunoResearch	Cat: 115-035-003, RRID:AB_10015289
Goat anti-rabbit IgG peroxidase-conjugated	Jackson ImmunoResearch	Cat: 111-035-003, RRID:AB_2313567
Donkey Anti-Sheep IgG peroxidase-conjugated	Jackson ImmunoResearch	Cat: 713-035-147, RRID:AB_2340710
Mouse anti-FLAG	Invitrogen	Cat: MA1-91878-1MG, RRID:AB_2537619
Goat anti-mouse-AlexaFluor-488	Invitrogen	Cat: A11001, RRID:AB_2534069
Chemicals, peptides, and recombinant proteins		
QIAamp viral RNA mini kit	QIAGEN	52904
2019-nCoV RUO kit	IDT	10006713
Positive template control (PTC) plasmid	IDT	10006625
TaqPath 1-Step RT-qPCR master mix	Thermo Fisher Scientific	A15300
SuperScript IV reverse transcriptase	Thermo Fisher Scientific	18090010
R9.4.1 flow cells	Nanopore Technologies	FLO-MIN106
AMX, LNB, SFB, EB and SQB	Nanopore Technologies	SQK-LSK109
Flow cell priming kit	Nanopore Technologies	EXP-FLP002
NEBNext Ultra II end-prep	New England Biolabs	E7546S
NEBNext quick ligation module	New England Biolabs	E6056S
Native barcoding expansion kits	Nanopore Technologies	EXP-NBD104, EXP-NBD114
Q5 high-fidelity DNA polymerase	New England Biolabs	M0491S
DNA clean & concentrator kit	Zymo Research	D4005
Lipofectamine 3000	Invitrogen	L3000-015
Pierce ECL western blotting substrate	ThermoFisher Scientific	#32106
X-Ray film	Santa Cruz Biotech	sc-201696
IFN-α2b	InvivoGen	rcyc-hifna2b
Luciferase assay system	Promega	E1500

(*Continued on next page*)

Continued

REAGENT or RESOURCE	SOURCE	IDENTIFIER
Type I interferon response (SAB Target List) H96 qPCR array	Bio-Rad	N/A
SsoAdvanced universal SYBR green supermix	Bio-Rad	1725270
Deposited data		
URLs for SARs-CoV-2 genome sequences are listed in the Table S1	GenBank	N/A
Oligonucleotides		
The oligonucleotides used in this study are listed in the Table S3	IDT	N/A
Software and algorithms		
SDS software v1.4	Applied Biosystems	4379633
RStudio v1.2.1335	The R project	https://www.r-project.org/
artic-ncov2019	ARTIC network	https://artic.network/ncov-2019
MinKNOW software	Oxford Nanopore Technologies	https://community.nanoporetech.com/protocols/experiment-companion-minknow/v/mke_1013_v1_revbm_11apr2016
PrimePCR analysis software	Bio-Rad	https://www.bio-rad.com/en-us/category/qpcr-analysis-software?ID=42a6560b-3ad7-43e9-bb8d-6027371de67a
CD-HIT	GitHub	https://github.com/weizhongli/cdhit
BioStrings	Bioconductor	https://bioconductor.org/packages/release/bioc/html/Biostrings.html
ggplot2	CRAN	https://cran.r-project.org/web/packages/ggplot2/index.html
Augur	Nextstrain	https://github.com/nextstrain/augur
Nextclade	Nextstrain	https://clades.nextstrain.org/
pangolin	Github	https://github.com/cov-lineages/pangolin
Trimal	Github	https://github.com/scapella/trimal
IQ-Tree	IQ-Tree	http://www.iqtree.org/
TreeTime	GitHub	https://github.com/jkanev/treetime
APE v5.3	CRAN	https://cran.r-project.org/web/packages/ape/index.html
tidyquant	CRAN	https://cran.r-project.org/web/packages/tidyquant/index.html
stats	CRAN	https://stat.ethz.ch/R-manual/R-devel/library/stats/html/00Index.html
UGENE	Unipro	http://ugene.net/

RESOURCE AVAILABILITY

Lead contact

Further information and requests for resources and reagents should be directed to and will be fulfilled by the lead contact, Blake Wiedenheft (bwiedenheft@gmail.com).

Materials availability

Plasmids generated in this study are available upon request from the lead contact.

Data and code availability

The complete SARS-CoV-2 genome sequences are deposited to GISAID EpiCoV and GenBank databases. GISAID accession IDs and URLs to GenBank records are provided in Table S1. Raw data for IFN response assay presented in Figures 3 and S3 is available in Table S2.

EXPERIMENTAL MODEL AND SUBJECT DETAILS

Cell cultures

HEK293T-hACE2 cells (BEI, NR-52511) were generously provided by Dr. Seth Pincus (Montana State University) and maintained at 37°C and 5% CO2 in Dulbecco's Modified Eagle Medium (DMEM, GIBCO, cat. #12100-061) supplemented with 10% fetal bovine serum (FBS, ATLAS Biologicals, Lot. #F31E18D1), sodium bicarbonate (3.7 g/L), 50 I.U./mL penicillin and 50 μg/mL streptomycin. Vero E6 cells (ATCC® cat. #CRL-1586) were maintained at 37°C and 5% CO2 in Eagle's Modified Eagle Medium (EMEM, ATCC®, cat. #30-2003) supplemented with 10% fetal bovine serum (FBS, ATLAS Biologicals, Lot. #F31E18D1) and 50 I.U./mL penicillin and 50 μg/mL streptomycin. All cell lines tested negative for mycoplasma.

Plasmids

Human-codon optimized dsDNA gene fragments (gBlocks) encoding for SARS-CoV-2 C-terminally FLAG-tagged ORF7aWT and ORF7aΔ115 proteins were synthesized by Integrated DNA Technologies (IDT). Sequence of ORF7a from Wuhan-Hu-1 reference (GenBank MN908947.3) was used for ORF7aWT gBlock. The gene fragments were cloned into the pEGFP-N1 (Clontech cat# 6085-1) backbone to replace the eGFP gene. pLV-mCherry was a gift from Pantelis Tsoulfas (Addgene plasmid # 36084; http://www.addgene.org/36084/; RRID:Addgene_36084).

Antibodies

Western blotting: Rabbit anti-ACTB (Cat: AC026, 1:20,000) antibodies were from ABclonal, Mouse anti-FLAG antibodies (Cat: MA1-91878-1MG, 1:1000) were from ThermoFisher Scientific, sheep anti-ORF7b antibodies (1:120) were from MRC I PPU, College of Life Sciences, University of Dundee, Scotland; Goat anti-mouse IgG peroxidase-conjugated (Cat: 115-035-003, 1:10,000), Goat anti-rabbit IgG peroxidase-conjugated (Cat: 111-035-003, 1:10,000) and Donkey Anti-Sheep IgG peroxidase-conjugated (Cat: 713-035-147, 1:10,000) antibodies were from Jackson ImmunoResearch. Immunocytochemistry: Mouse anti-FLAG antibodies (Cat: MA1-91878-1MG, 1:200), Goat anti-mouse-AlexaFluor-488 (Cat: A11001, 1:2,000) antibodies were from Invitrogen.

Human clinical sample collection and preparation

Clinical samples were obtained with local IRB approval (protocol #DB033020) and informed consent from patients undergoing testing for SARS-CoV-2 at Bozeman Health Deaconess Hospital. Patients tested for SARS-CoV-2 included both in-patients and out-patients. The latter included individuals who developed symptoms and sought medical care and asymptomatic (at the time of testing) individuals who were exposed to known COVID-19 case and therefore were tested. Nasopharyngeal swabs from patients that tested positive for SARS-CoV-2 were collected in viral transport media. RNA was extracted from all patient samples using QIAamp Viral RNA Mini Kit (QIAGEN) a biosafety level 3 (BSL3) laboratory. All samples were heat-inactivated before removing from BSL3. Information about age and sex of the patients is provided in Table S1.

Production and titration of coronavirus stocks

The nasopharyngeal swabs in the viral transport media were used to generate viral stocks as previously described (Harcourt et al., 2020). Briefly, 100 ul of the viral transport media was two-fold serially diluted and applied to Vero E6 cells When infected cells showed extensive cytopathic effect, the media was collected and utilized to generate a greater volume second passage in Vero E6 cells. When CPE was apparent, supernatants were centrifuged 1,000 RCF for 5 minutes to remove cellular debris. Virus titer in clarified supernatants was determined with plaque assay in Vero E6 cells as described (Loveday et al., 2021). For plaque assay, Vero E6 cells were incubated with viral inoculum at limiting dilutions. Inoculated cells were overlayed with either 0.75% methylcellulose, DMEM supplemented with 2% FBS and 1% pen-strep and incubated for 4 days. Cells were fixed and stained with 0.5% methylene blue in 70% ethanol. Plaques were counted and the overall titer was calculated. Viral stock's identity was confirmed via whole genome sequencing on Oxford Nanopore. All SARS-CoV-2 experiments were performed in a BSL3 laboratory.

Symptom onset data and clinical test results

Suspect cases of COVID-19 were tested in a CLIA lab and instructed to self-quarantine until notified of the RT-qPCR test results. All laboratory confirmed positive cases of COVID-19 were contacted via telephone by local public health nurses to complete contact tracing. During this interview, the nurses collected recorded symptoms, symptom onset date, travel history, contact with other known laboratory confirmed cases, close contacts and activities on the two days before symptom onset up until notification of a positive test. Data collection was conducted as part of a public health response. The study was reviewed by the Montana State University Institutional Review Board (IRB) For the Protection of Human Subjects (FWA 00000165) and was exempt from IRB oversight in accordance with Code of Federal regulations, Part 46, section 101. All necessary patient/participant consent has been obtained and the appropriate institutional forms have been archived.

CellPress
OPEN ACCESS

METHOD DETAILS

Quantitative reverse transcription PCR (qRT-PCR)

qRT-PCR was performed using CDC primers (N1 and N2) and probes from the 2019-nCoV RUO Kit (IDT# 10006713). SARS-CoV-2 RNA was quantified using one-step qRT-PCR in ABI 7500 Fast Real-Time PCR System according to CDC protocol (https://www.fda.gov/media/134922/download). In brief, 20 μL reactions included 8.5 μL of Nuclease-free Water, 1.5 μL of Primer and Probe mix (IDT, 10006713), 5 μL of TaqPath 1-Step RT-qPCR Master Mix (ThermoFisher, A15299) and 5 μL of the template. Nuclease-free water was used as negative template control (NTC). Amplification was performed using following program: 25°C for 2 min, 50°C for 15 min, 95°C for 2 min followed by 45 cycles of 95°C for 3 s and 55°C for 30 s. Run data was analyzed in SDS software v1.4 (Applied Biosystems). The NTC showed no amplification throughout the 40 cycles of qPCR.

RT-PCR and SARS-CoV-2 genome sequencing

For sequencing 10 μL of RNA from SARS-CoV-2 positive patient sample was reverse transcribed using SuperScript IV (Thermo Fisher Scientific) according to the supplier's protocol. The protocol developed by ARTIC Network was used to generate and sequence amplicon library that covers whole SARS-CoV-2 genome on Oxford Nanopore using ligation sequencing kit (SQK-LSK109) (https://artic.network/ncov-2019) (Grubaugh et al., 2019; Tyson et al., 2020). Briefly, two multiplex PCR reactions were performed with primer pools from ARTIC nCoV-2019 V3 Panel (IDT; Table S3) using Q5 High-Fidelity DNA Polymerase (New England Biolabs). Reactions were performed with the following thermocycling conditions: 98°C for 2min, 30 cycles of 98°C for 15 s and 65°C for 5 min. Two resulting amplicon pools for each patient sample were combined and used for library preparation. After end repair (NEB E7546) samples were barcoded using Native Barcoding Expansion Kits EXP-NBD104 and EXP-NBD114 from Oxford Nanopore. A total of 24 barcoded samples were pooled together and Nanopore adaptors were ligated. After clean-up 20 ng of multiplexed library DNA was loaded onto the MinION flowcell for sequencing. A total of 0.3 Gb of raw sequencing data was collected per patient sample. Nuclease-free water was used as a negative control for library preparation and sequencing. Non-specific amplification in negative control was additionally checked using an agarose gel. SARS-CoV-2 Isolate USA-WA1/2020 (BEI, NR-52281) was used as a positive control for genome sequencing.

SARS-CoV-2 genome assembly

MinKNOW software was used to basecall raw Nanopore reads in high-accuracy mode. ARTIC bioinformatic pipeline for COVID-19 was used to analyze reads (https://artic.network/ncov-2019). Pipeline included demultiplexing with guppy barcoder and generating consensus sequences with minimap2 and calling single nucleotide variants with nanopolish relative to Wuhan-Hu-1/2019 reference genome (Li, 2018; Quick et al., 2017; Wu et al., 2020). 20X coverage was used as a threshold both for consensus and variant calling. Nucleotide positions with less than 20X coverage were masked with Ns in the final consensuses. Consensus sequences were uploaded to GISAID (https://www.gisaid.org/), accession IDs are provided in Table S1.

RT-PCR and Sanger sequencing

To verify the ORF7aΔ115 mutation we used RT-PCR with primers that flank the deletion region (Table S3). Reactions were performed with Q5 High-Fidelity DNA Polymerase in 25 μL volume (New England Biolabs) using following program: 98°C for 2min, 35 cycles of 98°C for 15 s and 65°C for 5 min, 35 cycles. PCR products were analyzed on 1% agarose gels stained with SYBR Safe (Thermo Fisher Scientific). The remaining volume of the reaction was purified using DNA Clean & Concentrator kit (Zymo Research) and sent to Psomagen for Sanger sequencing. Each PCR product was sequenced with both forward and reverse primers used for PCR. To detect sgRNAs of ORF7a and ORF7b primers annealing to Leader region of SARS-CoV-2 and inside the ORF were used (Table S3). PCR products were cut out from 1% agarose gel and purified with Zymoclean Gel DNA Recovery Kit. Purified products were sequenced with forward and reverse primers. Sequence was verified by aligning to SARS-CoV-2 genome in UGENE software (Unipro).

Phylogenetic and ORF7a mutational analysis

An alignment of 181,003 SARS-CoV-2 genomes was downloaded from the GISAID database at 9:11 AM on 2020-11-11, and sequences without corresponding metadata entries were removed. The nucleotide positions encoding ORF7a in the reference sequence (Wuhan-Hu-1; EP_ISL_402125) were extracted for the remaining 180,971 sequences, and ORF7a sequences with 100% sequence identity were clustered using CD-HIT (with settings: -c 1 -aL 1). One representative was randomly selected from each of the 846 ORF7a sequence clusters and mutations in each nucleotide and translated sequence were determined using the Biostrings package in R. Graphs of these mutations were rendered with the ggplot2 package. To construct a phylogenetic tree of global and Bozeman SARS-CoV-2 sequences, up to ten sequences from each country in the world were selected for each month of the pandemic using the Filter utility in the Augur pipeline (–group-by country year month–sequences-per-group 10) (Bedford et al., 2020; Lemieux et al., 2021). This resulted in an alignment of 4,235 GISAID sequences. Then, the Nextclade online tool was used to determine the quality of 73 SARS-CoV-2 genomes (% genome covered) sequenced from Bozeman patients. 55 Bozeman sequences that were determined to be of "Good" quality were merged with the alignment of GISAID sequences, as well as an alignment of 669 representative SARS-CoV-2 genomes that had non-synonymous mutations in ORF7a. The bat coronavirus RaTG13 (MN996532.2) and the Wuhan- Hu-1 SARS-CoV-2 sequences were also merged, resulting in an alignment of 4,959 full genome

sequences, and positions that are hypervariable or prone to sequencing artifacts were masked with a VCF file downloaded from EMBL at 12:45PM on 2020-05- 29. The alignment was trimmed of columns composed of 90% or more gaps using Trimal (-gt 0.9), and IqTree was used to construct a maximum likelihood phylogeny (-m GTR -ninit 2 -n 2 -me 0.05). Branch lengths and internal nodes were rescaled on the resulting tree using TreeTime, and tree was re-rooted to the RaTG13 sequence using the APE package before being visualized with the ggTree package in R. Clades were assigned to SARS-CoV-2 genomes using Nextclade and pangolin (https://cov-lineages.org/) utilities.

Western blot

293T-hACE2 cells were transfected using Lipofectamine 3000 (Invitrogen, L3000-015) with plasmids encoding for ORF7aWT, ORF7aΔ115 or control pEGFP-N1 plasmid. To detect ORF7b expression cells were infected with ORF7aWT or ORF7aΔ115 SARS-CoV-2 strains at MOI = 0.05. After 24 hours, cells were washed two times with PBS and lysed in RIPA buffer (150 mM sodium chloride, 1% NP-40, 0.5% sodium deoxycholate, 0.2% SDS, 50 mM Tris, pH 8.0) at 4°C for 30 min. The lysates were clarified by centrifugation (10'000 g, 20 min) and stored at −80°C. For western blot lysates were mixed with 6xLaemmli SDS-PAGE buffer and heated at 98°C for 5 min, resolved in 12% SDS-PAGE gel and transferred onto a PVDF (ORF7b) or nitrocellulose (ORF7a) membrane using Mini Trans-Blot Electrophoretic Transfer Cell (Bio-Rad, #1703930). Membranes were blocked and probed with indicated antibodies. The proteins were visualized using Pierce ECL Western Blotting Substrate (ThermoFisher Scientific, #32106) and exposed to X-Ray film (sc-201696, Santa Cruz Biotech).

Immunocytochemistry

HEK293T-hACE2 were transfected with plasmid DNA using Lipofectamine 3000 (Invitrogen REF: L3000-015) according to manufacturer's instructions. Cells were either transfected with expression vectors for SARS-CoV-2 ORF7aWT, SARS-CoV-2 ORF7aΔ115, or mock transfected. 24 hours after transfection, cells were detached and seeded at 50% confluency on glass coverslips (Fisherbrand, #12-545-80) pre-coated with poly-D-lysine (Cultrex, #3439-100-01) in a 24 well plate. The next day, media was removed, and cells were washed with PBS and fixed with ice-cold 100% methanol on ice for 10 minutes. Half of the methanol was replaced with PBS three times before the methanol solution was discarded and cells were washed three times in PBS (5 minutes each wash). Cells were blocked with 1% BSA (Fisher Scientific BP9703-100) in PBS + 0.1% Tween-20 (PBST) for 30 minutes at room temperature. After blocking, cells were stained with mouse monoclonal anti-Flag antibody (Invitrogen, MA1-91878) (1:200 in 1% BSA in PBST) overnight at 4°C. The next day, cells were washed 3X in PBS (5 min each) and stained with secondary antibody diluted 1:2000 in 1% BSA in PBST for 1 h at RT in the dark (Goat anti-mouse AlexaFluor488; Invitrogen, A11001). After 3x PBS washes nuclei were stained with Hoechst 33342 in PBS for 5 minutes at RT. Coverslips were then mounted with ProLong Gold antifade mounting media (Invitrogen, P36934) on Superfrost Plus microscope slides (#22-037-246). Immunostained cells were imaged using a Leica SP8 confocal microscope.

IFN inhibition assay

To generate ISRE reporter system, HEK293T cells were transduced with lentiviruses carrying pGreenFire1-ISRE (Cat. TR016PA-1, SBI) construct and selected with puromycin (1 ug/ml) for 2 days. After selection cells (1x105 cells/well, 48-well plate) were transfected with expression plasmids (250 ng) for SARS-CoV-2 ORF7aWT, SARS-CoV-2 ORF7aΔ115, or control plasmid pLV-mCherry. 16 hours post transfection, cells were treated for 24 h with 5 ng/ml of human IFN-α2b (Cat. rcyc-hifna2b, InvivoGen) according to manufacturer's recommendations. After treatment activation of IFN signaling was measured using Luciferase Assay System (Cat. E1500, Promega) on Cytation 5 (BioTek) plate reader. Assay was performed in six replicates for each condition.

SARS-CoV-2 replication assays

HEK293T-hACE2 and Vero E6 cells were seeded in the 48-well plate and infected with ORF7aWT or ORF7aΔ115 SARS-CoV-2 strains at MOI = 0.05 in 50 μL of the cell culture media. Infections were performed in triplicates. Next, 0.5 h post infection (hpi) 500 μL of the fresh cell culture media was added to each well. The supernatants (140 ul) from the infected cells were harvested at the following time points 0.5, 6, 24, 48, 72 and 120 hpi. The RNAs from the supernatants were extracted using QIAamp Viral RNA Mini Kit (QIAGEN) and used as an input in qRT-PCR with CDC N1 and N2 primers and probes as described above. Relative quantification was used (ΔCt method) to calculate viral replication versus 0.5 hpi time point as 2-ΔCt.

The infected cells were harvested 0.5, 6 and 24 hpi and washed with PBS. Total RNA from cells was extracted using RNeasy kit (QIAGEN, Cat No./ID: 74104) with on-column DNase digestion step (QIAGEN, 79254) according to the manufacturers protocol. Viral RNA was quantified using qRT-PCR CDC N1 primers and probe. Human ACTB endogenous control was quantified with TaqMan assay (ThermoFisher, 4333762T). ΔΔCt method was used to normalize viral RNA level to host RNA and 0.5 hpi. Viral replication was calculated for each replicate as 2-ΔΔCt.

Type I interferon response assay

HEK293T-hACE2 were seeded in the 48-well plate and infected with ORF7aWT or ORF7aΔ115 SARS-CoV-2 strains at MOI = 0.05 in 50 ul of the media. After 30 min on infection the 500 μL of the cell culture media was added to each well. At 24 hpi the cells were washed once with PBS, detached using Trypsin and the total RNA was extracted using RNeasy kit (QIAGEN, Cat No./ID: 74104)

with on-column DNase digestion (QIAGEN, Cat No./ID: 79254) according to the manufacturer's protocol. Non-infected cells were processed using the same protocol with mock infection. After extraction, 0,5-1 μg of total RNA was reverse transcribed Reverse using SuperScript IV Reverse Transcriptase (Thermo Fisher Scientific) according to the supplier's protocol. The cDNA was diluted 10-fold in water and analyzed with Type I interferon response (SAB Target List) H96 qPCR array. Each reaction contained 2 μL of cDNA, 10 μL of 2X SsoAdvanced Universal SYBR Green Supermix (Bio-Rad) and 8 μL of water. Reactions were performed on QuantStudio 3 Real-Time PCR System instrument with following thermocycling conditions: 95°C for 2min, 40 cycles of 95°C for 5 s and 60°C for 30 s. After amplification, melt curve analysis was performed to examine product specificity. Assay was performed in triplicates for non-infected cells and both viruses. Run data was analyzed in PrimePCR Analysis software (Bio-Rad). Expression of IFN-I response genes was normalized to geometric mean of 3 reference transcripts (TBP, GAPDH, HPRT1) and non-infected control (ΔΔCt method).

QUANTIFICATION AND STATISTICAL ANALYSIS

All statistical analyses were performed in RStudio v1.2.1335. Moving averages ($n = 7$) for symptom onset and positive COVID-19 tests data were calculated using geom_ma function from tidyquant package and plotted with ggplot2 in RStudio. qRT-PCR data is shown as mean of three biological replicates (each with three technical replicates) ± standard deviation (SD). Data in ISRE reporter assay was analyzed with one-way ANOVA with Tukey's post hoc pairwise comparisons. Replication of viruses and expression of IFN-I response genes was compared using Student's t test. Medians of IFN-I response between two viruses were compared with Wilcoxon signed-rank test. Significance levels in figures: * $p < 0.05$, ** $p < 0.01$, *** $p < 0.001$ or ns (no significant difference, $p > 0.05$).